

Supporting Information

Ultrafast Study of Substituted-Position-Dependent Excited-state Evolution in Benzophenone-Carbazole Dyads

Jiayu Li,^[a] Sirui Yang,^[a,b] Ziqi Deng,^[a,c] Shaofei Ni,^[a] Shunli Chen,^[a] Li Dang,^{*[a,b]}
Ming-De Li^{*[a,b]}

^[a] J. Li, S. Yang, Z. Deng, Dr. S. Ni, Dr. S. Chen, Prof. L. Dang, Prof. M.-D. Li

Department of Chemistry and Key Laboratory for Preparation and Application of Ordered Structural Materials of Guangdong Province, Shantou University, Guangdong 515063, P. R. China.

^[b] S. Yang, Prof. L. Dang, Prof. M.-D. Li

Chemistry and Chemical Engineering Guangdong Laboratory, Shantou 515031, P. R. China.

^[c] Z. Deng

Department of Chemistry, The University of Hong Kong, Hong Kong SAR, P.R. China

Contents

Instruments and experiment methods	S2
Synthesis and characteristic	S4
UV-Vis absorption and photoluminescence spectra	S9
Femtosecond and nanosecond transient absorption (fs-TA and ns-TA) spectra	S11
Theoretical calculations	S19
References	S20

1. Instruments and experiment methods

(1) Materials

All the materials used in synthesis were purchased from Energy chemical. Solvents include Tetrahydrofuran (THF), Dichloromethane (DCM), Dimethyl formamide (DMF) and Dimethyl Sulfoxide (DMSO) were purchased from J&K. All the materials were used without further purification.

(2) Instruments

The ^1H NMR spectra were measured using Zhongke Niujin WNMR-I 400 spectrometer with tetramethylsilane (TMS; $\delta = 0$) as the internal reference. High resolution mass spectra (HRMS) were recorded using a Thermo Q Exactive spectrometer. UV-Vis absorption and photoluminescence measurements were performed with UV-Vis spectrophotometer (SHIMADZU® UV-1780) and Fluorescence spectrometer (PTI® QM-TM).

(3) Femtosecond transient absorption (fs-TA) experiments

The fs-TA measurements were performed based on a femtosecond Ti: Sapphire regenerative amplifier laser system (Coherent, Astrella-Tunable-F-1k) and femtosecond transient absorption spectrometer system (Ultrafast Systems, Helios Fire). The laser probe pulse was produced with ~4% of the amplified 800 nm laser pulses to generate a white-light continuum (320–800 nm) in a CaF_2 crystal and then this probe beam was split into two parts before traversing the sample. One probe laser beam goes through the sample while the other probe laser beam goes to the reference spectrometer to monitor the fluctuations in the probe beam intensity. The instrument response function was determined to be ca. 120 fs. At each temporal delay, data were averaged for 2 s and collected by the acquisition system. For the experiments described in this study, the sample solution was excited by a 340 nm pump beam with a power of 0.2 mW (from TOPAS). The sample solutions were excited in a 2 mm path-length cuvette. The data were stored as three-dimensional (3D) wavelength-time-absorbance matrices that were exported for use with the fitting software. Chirp correction was done for all the data shown here. The kinetics of all fs-TA spectra were fitted by single-wavelength

fitting via Surface Explorer software; all the error values were shown with 90% confidence intervals.

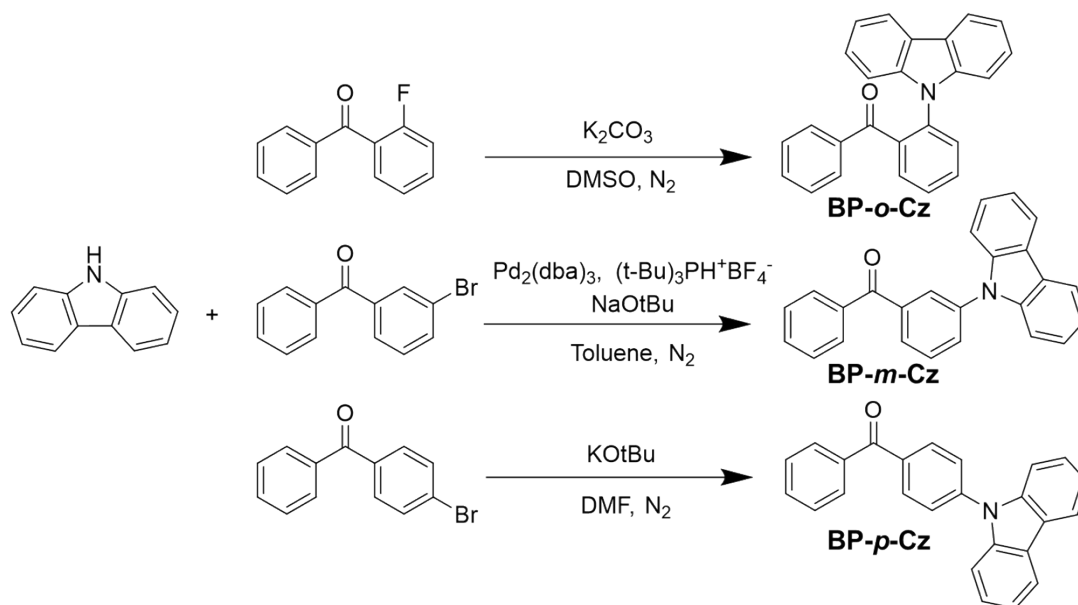
(4) Nanosecond transient absorption (ns-TA) experiments

The ns-TA measurements were performed by using a nanosecond pulsed probe light source, a photonic crystal fiber (PCF)-based supercontinuum laser. The pulse duration of this probe determines the time resolution of the spectrometer (<1 ns). In ns-TA, the pump-probe delay is controlled electronically, and the maximum time window is very close to half the repetition period of the pump laser. In our case, the maximum time window is 400 μ s. The excited wavelength and sample solutions employed in the ns-TA experiments were the same as the fs-TA's. The data were stored as three-dimensional (3D) wavelength-time-absorbance matrices that were exported for use with the fitting software. The kinetics of all ns-TA spectra were fitted by single-wavelength fitting via Surface Explorer software; all the error values were shown with 90% confidence intervals.

(5) Theoretical calculations

Density functional theory (DFT) and time-dependent density functional theory (TD-DFT) are applied to calculate the optimized geometries and electronic structures of the ground state (S_0) and the excited state (S_n) of BP-Cz dyads. CAM-B3LYP/6-311G** through the Gaussian 16 program package¹ is employed to optimize the structure, calculate energy levels and reveal the characteristics of the hole and electron of S_1 and S_2 . Multiwfn program² is used to analyze and visualize hole-electron distribution, transition density, Δr index and intramolecular interaction (Independent gradient model, IGM). VMD software³ is used to obtain a 3D isosurface of intramolecular interaction for *o*-BCz (Isosurface value=0.005). SOC constants are calculated based on ORCA program system⁴.

2. Synthesis and characteristic



Scheme S1. Synthetic routes to BP-Cz dyads

Synthesis of BP-*o*-Cz

Into a 100 ml two necked round-bottom flask were placed 2-fluorobenzophenone (1.10 g, 5.5 mmol), carbazole (5 g, 12 mmol), and Potassium carbonate (9 g, 65 mmol). The flask was evacuated under vacuum and flushed with dry nitrogen for three times. Then dry DMSO (30 mL) was injected. The mixture was heated to 180°C and stirred for 24 h, and then cooled to room temperature. The mixture was poured into water and extracted by DCM three times. The organic phase was washed with water three times and dried over sodium sulfate anhydrous. The crude product was further purified by flash chromatography (silica gel, PE/DCM, 7/1, v/v), obtaining a white solid in 62% yield (1.18 g). 1H NMR (400 MHz, $CDCl_3$) δ 7.92 (dd, $J = 7.6, 1.3$ Hz, 1H), 7.87 – 7.78 (m, 3H), 7.67 (dd, $J = 15.4, 7.7$ Hz, 2H), 7.37 (dd, $J = 11.3, 4.0$ Hz, 2H), 7.26 (d, $J = 8.2$ Hz, 2H), 7.18 (t, $J = 7.4$ Hz, 2H), 7.05 (d, $J = 7.1$ Hz, 2H), 6.99 (t, $J = 7.5$ Hz, 1H), 6.73 (t, $J = 7.8$ Hz, 2H). ^{13}C NMR (101 MHz, $CDCl_3$) δ 196.82, 140.92, 137.69, 136.48, 136.20, 132.59, 131.96, 131.25, 128.92, 128.34, 127.82, 126.94, 125.76, 123.22, 119.98, 119.93, 109.94. HRMS m/z : $[M+H]^+$ calcd for $C_{25}H_{18}NO$, 348.1388, found 348.1395

Synthesis of BP-*m*-Cz

Into a 100 ml two necked round-bottom flask were placed 3-bromobenzophenone (1.3 g, 5 mmol), carbazole (1 g, 6 mmol), Tris(dibenzylideneacetone)dipalladium (Pd₂(dba)₃, 0.7 g, 0.8 mmol), Tri-*tert*-butylphosphine tetrafluoroborate (0.7 g, 2.5 mmol) and sodium *tert*-butoxide (2.4 g, 25 mmol). The flask was evacuated under vacuum and flushed with dry nitrogen for three times. Then dry toluene (30 mL) was injected. The mixture was heated to 110°C and stirred for 24 h, and then cooled to room temperature. The mixture was poured into water and extracted by DCM three times. The organic phase was washed with water three times and dried over sodium sulfate anhydrous. The crude product was further purified by flash chromatography (silica gel, PE/DCM, 7/1, v/v), obtaining a white solid in 81% yield (1.41 g). ¹H NMR (400 MHz, CDCl₃) δ 8.17 (d, *J* = 7.8 Hz, 2H), 8.03 (s, 1H), 7.92 (dd, *J* = 10.6, 7.6 Hz, 3H), 7.85 (dd, *J* = 6.7, 1.8 Hz, 1H), 7.77 (t, *J* = 7.8 Hz, 1H), 7.63 (t, *J* = 7.4 Hz, 1H), 7.53 (t, *J* = 7.6 Hz, 2H), 7.49 – 7.41 (m, 4H), 7.37 – 7.30 (m, 2H). ¹³C NMR (101 MHz, CDCl₃) δ 195.76, 140.66, 139.61, 137.98, 137.17, 132.88, 130.89, 130.09, 130.04, 128.86, 128.52, 128.40, 126.17, 123.60, 120.48, 120.35, 109.60. HRMS *m/z*: [M+H]⁺ calcd for C₂₅H₁₈NO, 348.1388, found 348.1394

Synthesis of BP-*p*-Cz

Into a 100 ml two necked round-bottom flask were placed 4-bromobenzophenone (1.3 g, 5 mmol), carbazole (1 g, 6 mmol), and Potassium *tert*-butoxide (1.2 g, 11 mmol). The flask was evacuated under vacuum and flushed with dry nitrogen three times. Then dry DMF (30 mL) was injected. The mixture was heated to 150°C and stirred for 24 h, and then cooled to room temperature. The mixture was poured into water and extracted by DCM three times. The organic phase was washed with water three times and dried over sodium sulfate anhydrous. The crude product was further purified by flash chromatography (silica gel, PE/DCM, 7/1, v/v), obtaining a white solid in 65% yield (1.13 g). ¹H NMR (400 MHz, CDCl₃) δ 8.18 (d, *J* = 7.7 Hz, 2H), 8.14 – 8.07 (m, 2H), 7.97 – 7.90 (m, 2H), 7.76 (d, *J* = 8.4 Hz, 2H), 7.67 (t, *J* = 7.4 Hz, 1H), 7.60 – 7.53 (m, 4H), 7.51 – 7.43 (m, 2H), 7.35 (t, *J* = 7.4 Hz, 2H). ¹³C NMR (101 MHz, CDCl₃) δ

196.82, 140.92, 137.69, 136.48, 136.20, 132.59, 131.96, 131.25, 128.92, 128.34, 127.82, 126.94, 125.76, 123.22, 119.98, 119.93, 109.94. HRMS m/z: $[M+H]^+$ calcd for $C_{25}H_{18}NO$, 348.1388, found 348.1393

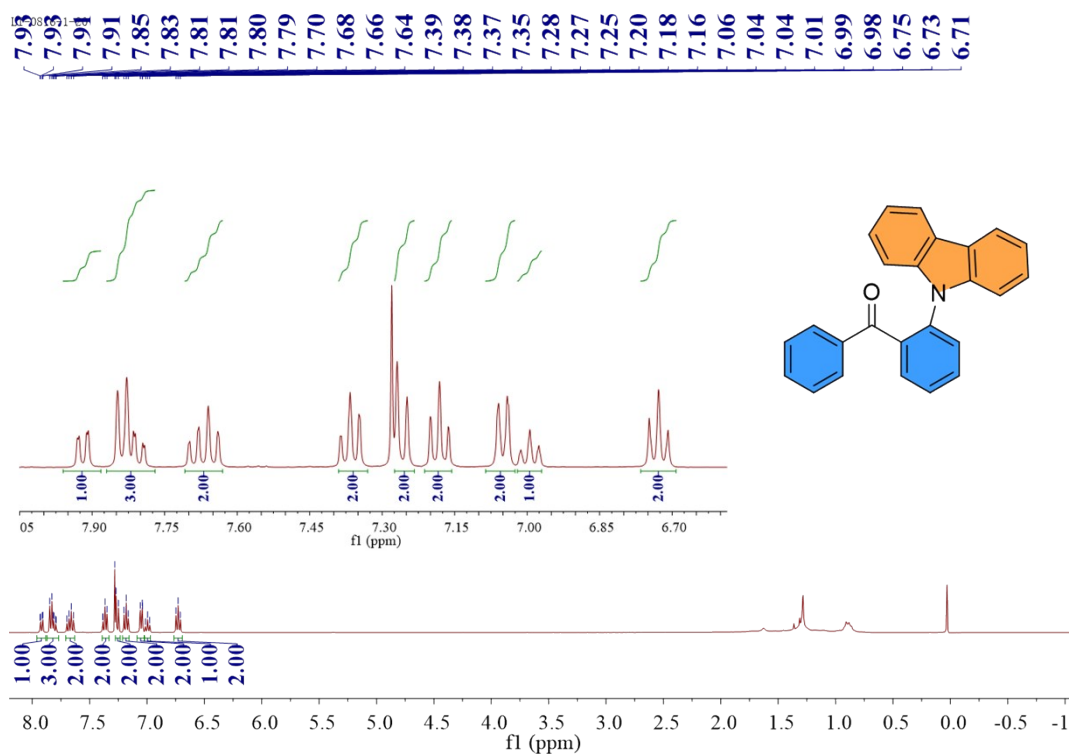


Figure S1. 1H NMR of BP-*o*-Cz

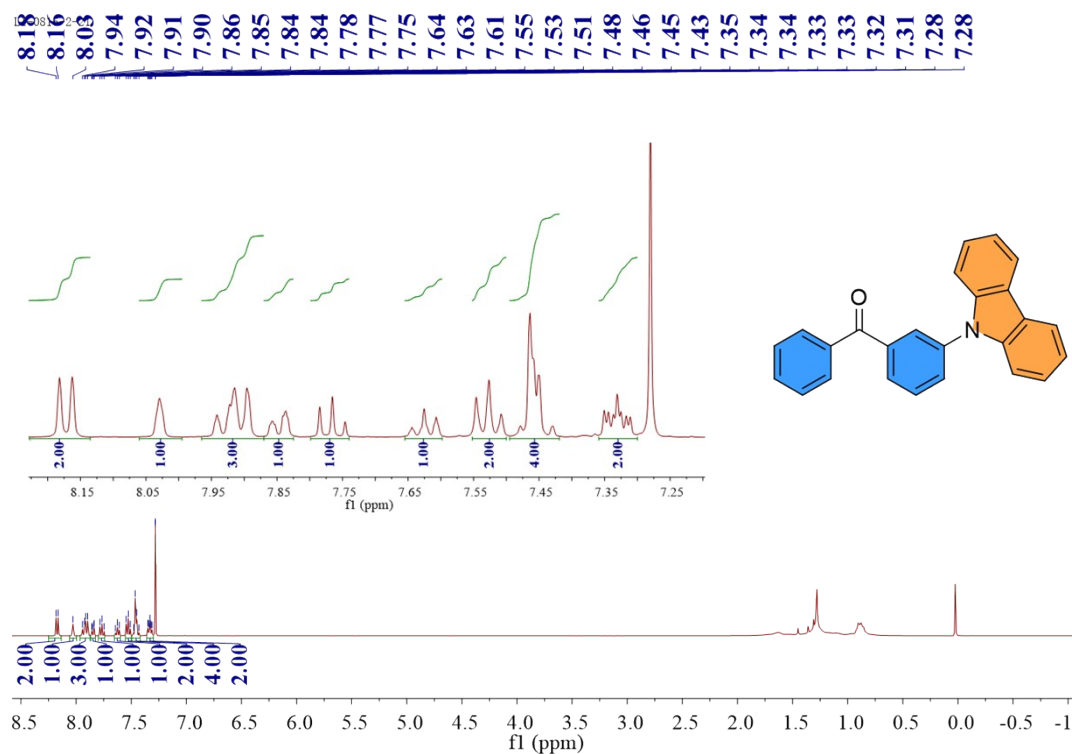


Figure S2. 1H NMR of BP-*m*-Cz

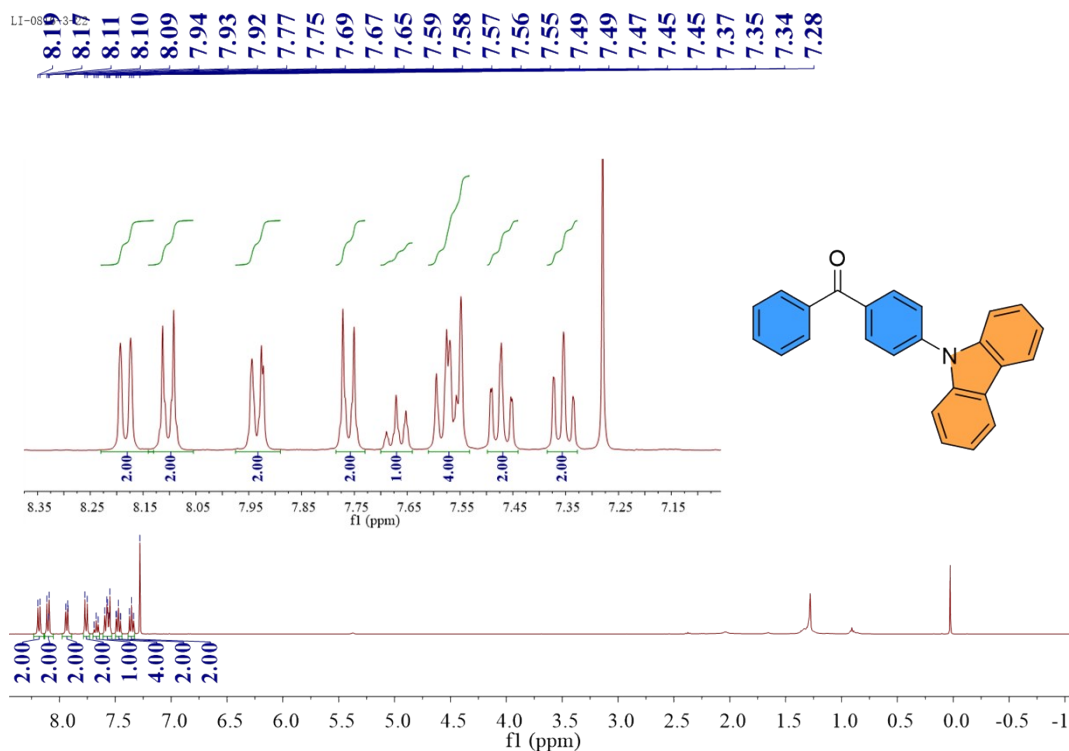


Figure S3. ^1H NMR of BP-*p*-Cz

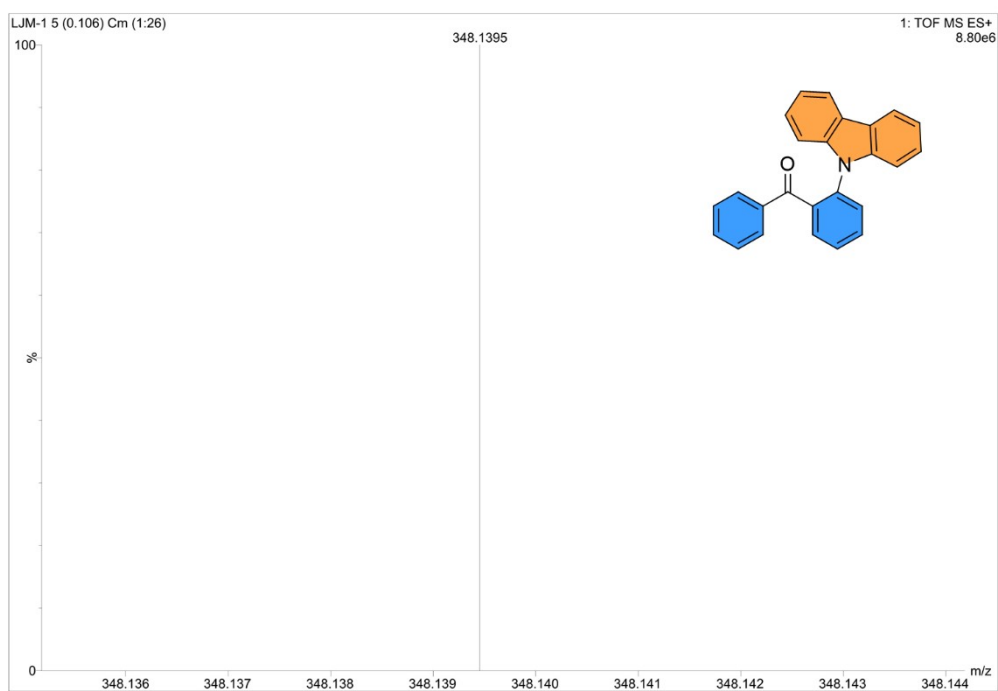


Figure S4. HRMS of BP-*o*-Cz

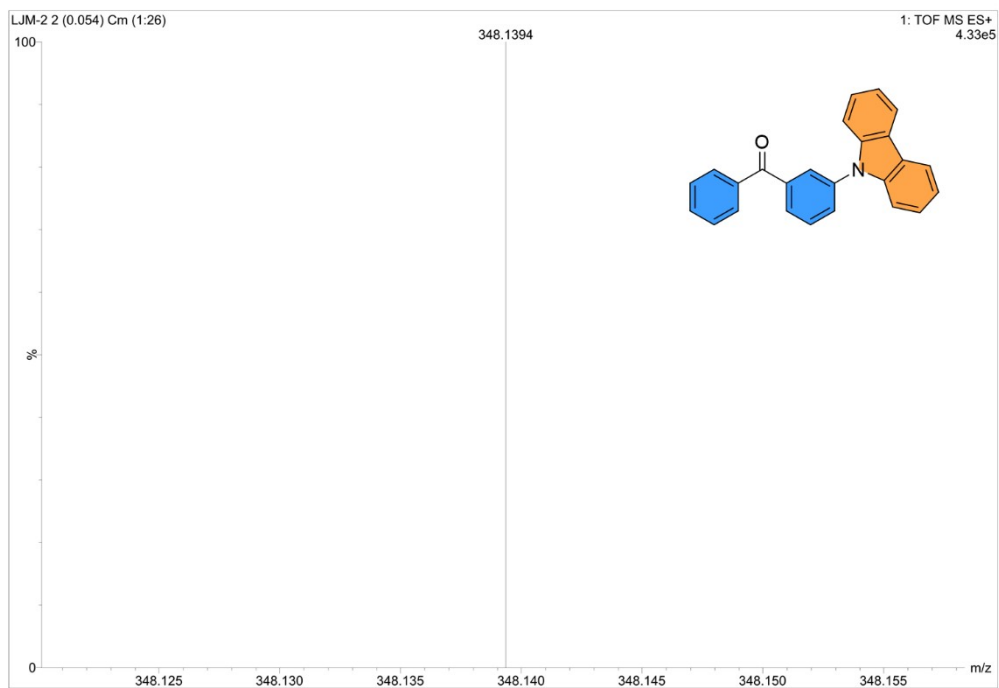


Figure S5. HRMS of BP-*m*-Cz

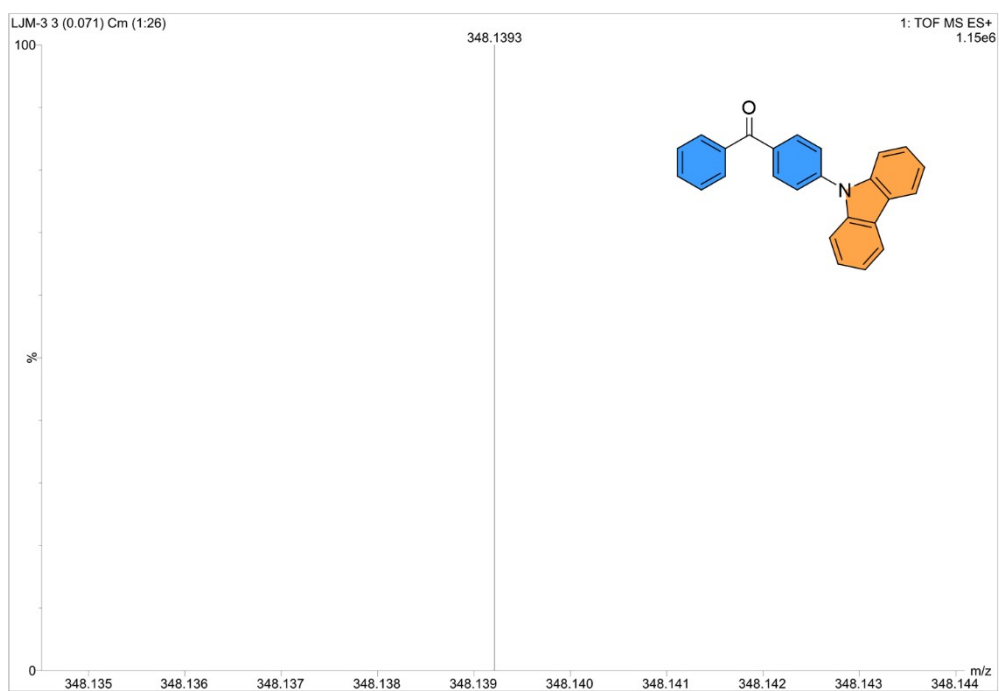


Figure S6. HRMS of BP-*p*-Cz

3. UV-Vis and PL spectra

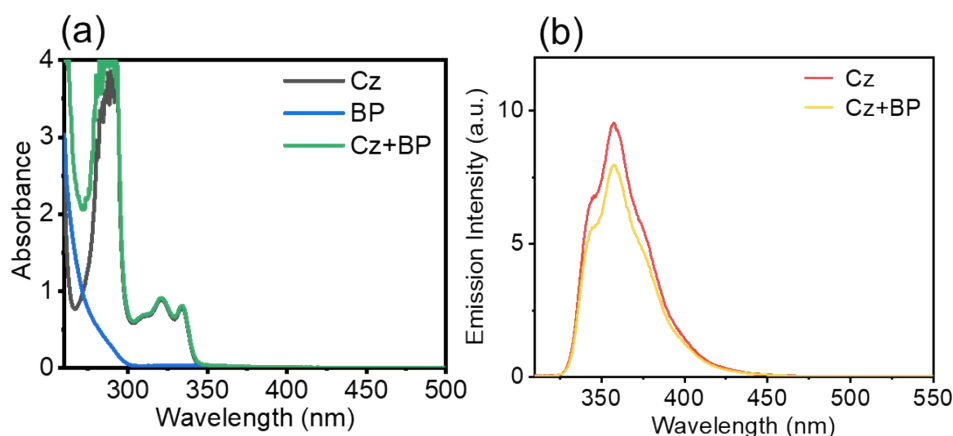


Figure S7. UV-vis spectra and FL spectra of BP, Cz and mix solution in ACN, 1 mM.

The Lippert-Mataga model

The Lippert-Mataga model is estimated according to equation 1.

$$hc(\nu_a - \nu_f) = hc(\nu_a^0 - \nu_f^0) + \frac{2(\mu_e - \mu_g)^2}{a_0^3} f(\epsilon, n) \quad \text{Eq 1}$$

where, $\mu_e - \mu_g$ ($\Delta\mu$) is the difference between the dipole moments of excited and ground states, c is the speed of light, h is Planck's constant, and a_0 is the radius of the Onsager cavity around the fluorophore and is considered to be half of the average molecular sizes of BP-Cz dyads. Solvent dielectric constant (ϵ) and refractive index (n) are included in the term f , known as the solvent polarity parameter. $\nu_a - \nu_f$ is the Stokes shift. The a_0 and μ_g were estimated but DFT calculation.

Table S1. Detail information of Lippert–Mataga model for BP-Cz dyads.

	a_0 (Å)	μ_g (D)	μ_e (D)	$\Delta\mu$ (D)
BP- <i>o</i> -Cz	6.036	2.56	12.02	9.45
BP- <i>m</i> -Cz	6.325	3.81	13.42	9.61
BP- <i>p</i> -Cz	8.563	2.64	18.29	15.65

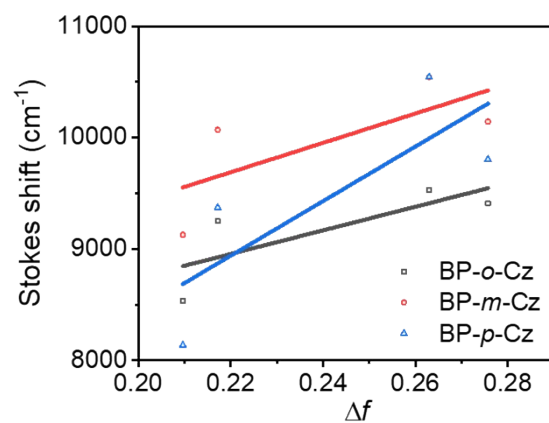


Figure S8. Lippert-Mataga plots for BP-Cz dyads.

Table S2. Fluorescence lifetime of BP-Cz compounds in different solvents.

	τ [ns]			
	THF	DCM	DMF	DMSO
BP- <i>o</i> -Cz	6.01	10.87	7.21	11.97
BP- <i>m</i> -Cz	5.20	16.91	15.85	15.61
BP- <i>p</i> -Cz	4.73	4.87	6.48	7.51

4. Femtosecond and nanosecond transient absorption spectra

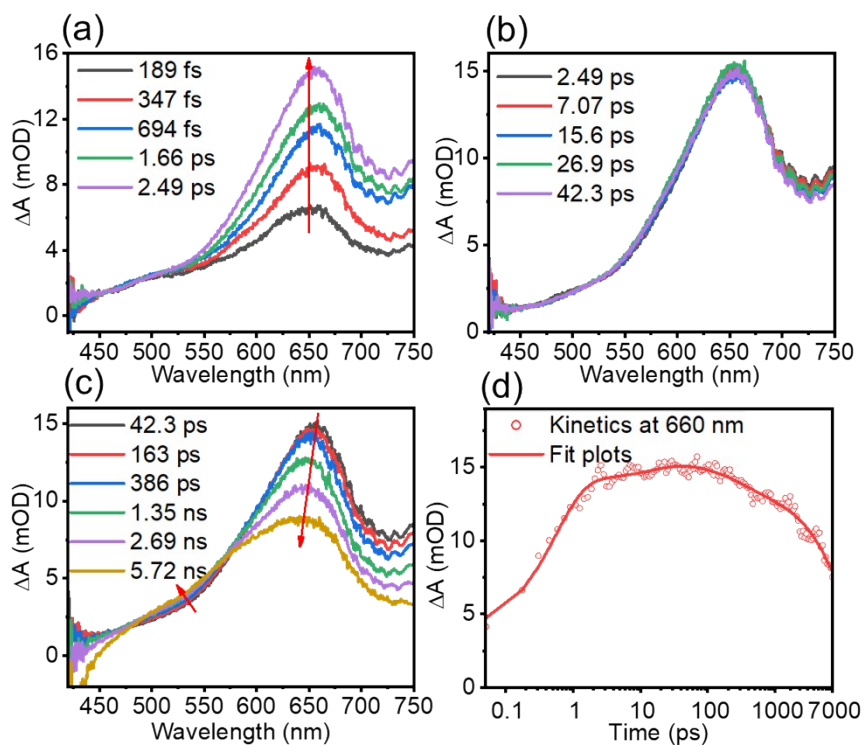


Figure S9. Fs-TA spectra of BP-*o*-Cz in THF, 0.1 mM

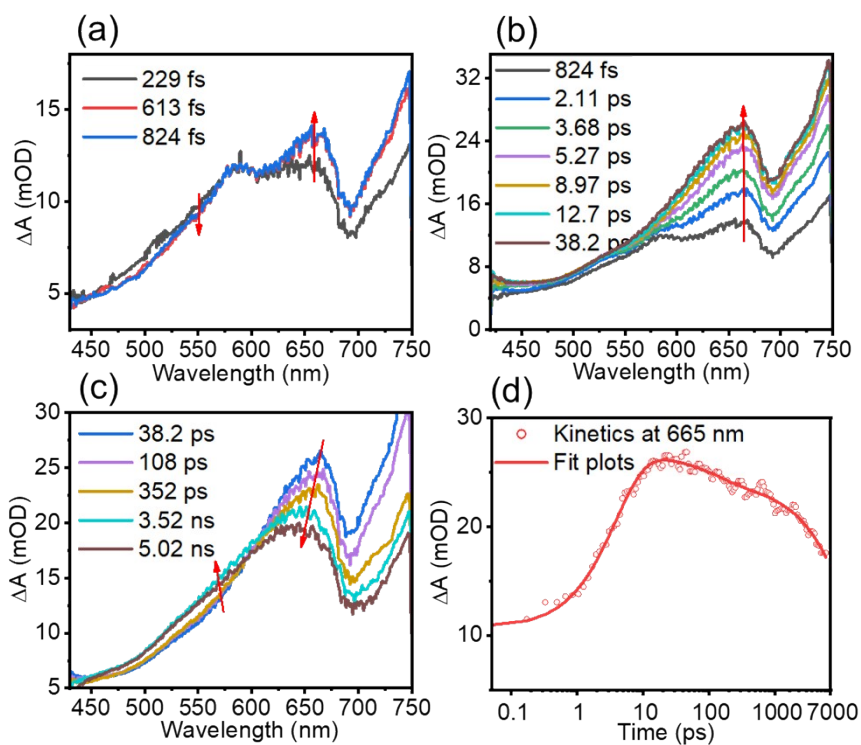


Figure S10. Fs-TA spectra of BP-*m*-Cz in THF, 0.1 mM

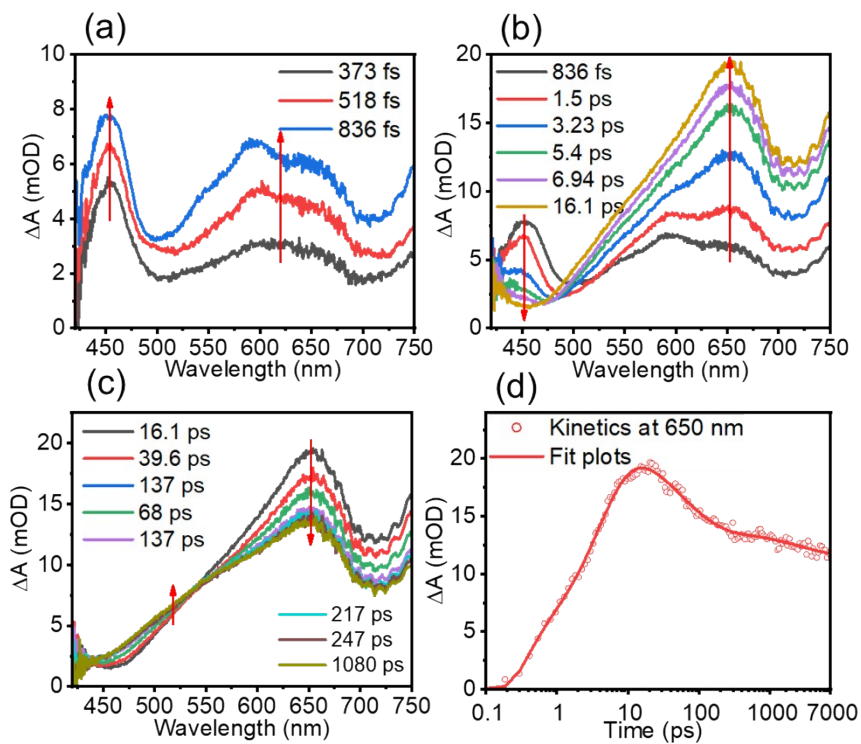


Figure S11. Fs-TA spectra of BP-*p*-Cz in THF, 0.1 Mm

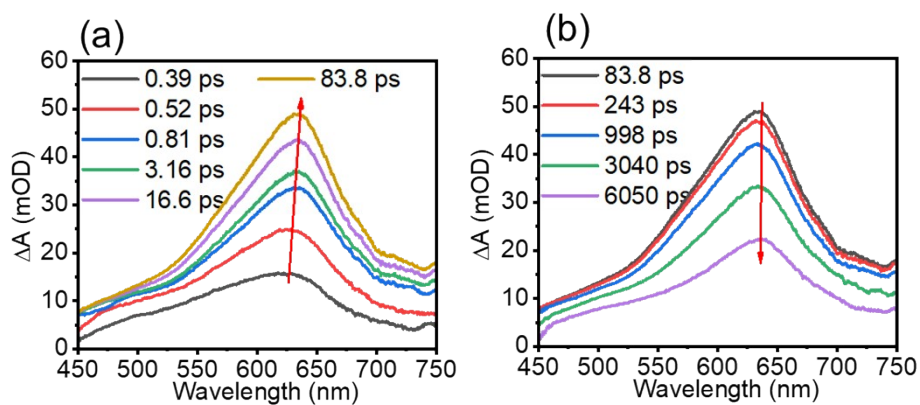


Figure S12. Fs-TA spectra of Cz in THF, 0.1 mM

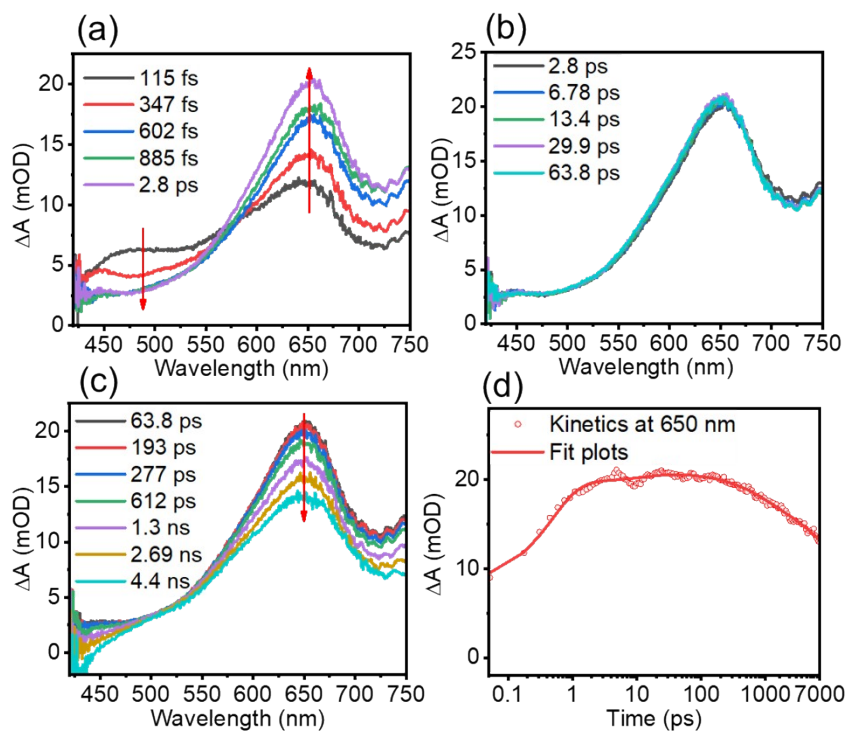


Figure S13. Fs-TA spectra of BP-*o*-Cz in DMF, 0.1 mM

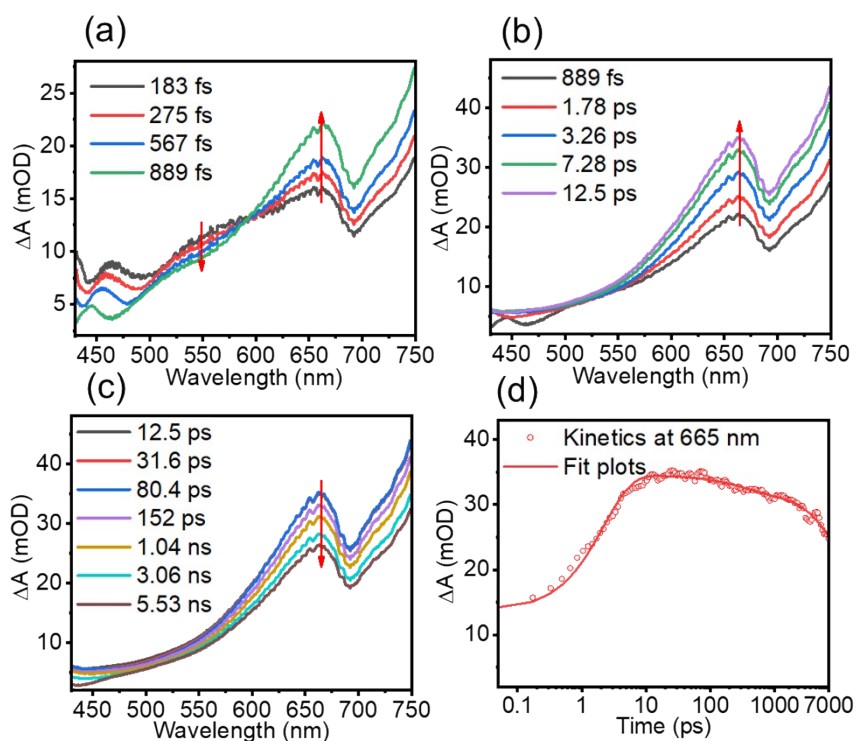


Figure S14. Fs-TA spectra of BP-*m*-Cz in DMF, 0.1 mM

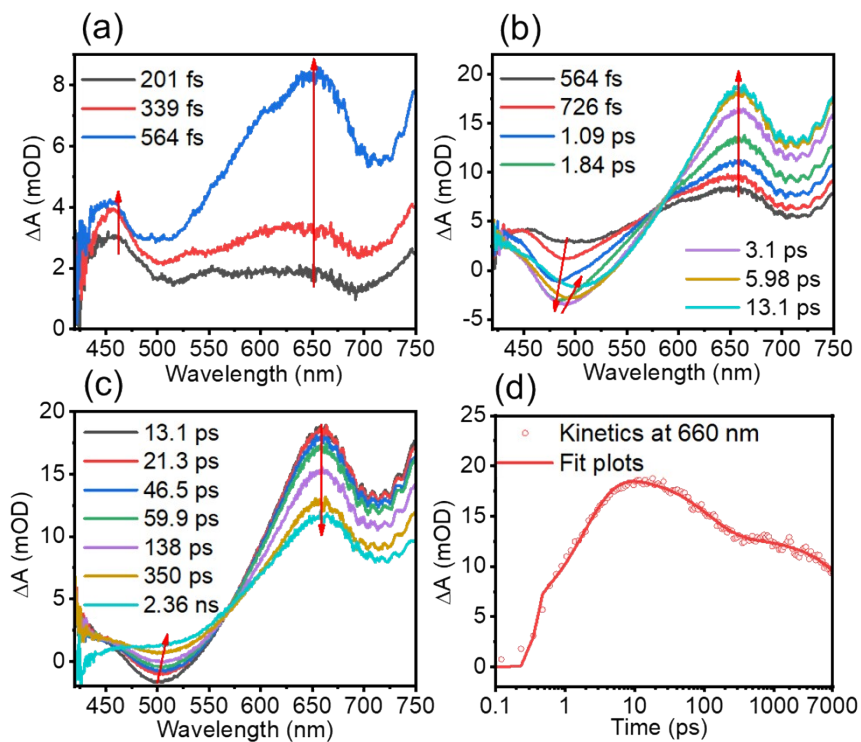


Figure S15. Fs-TA spectra of BP-*p*-Cz in DMF, 0.1 mM

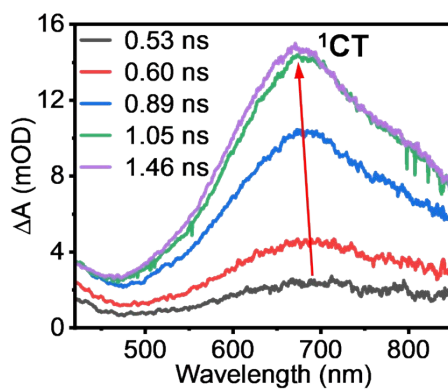


Figure S16. Ns-TA spectra of BP-*o*-Cz in THF, 0.1 mM

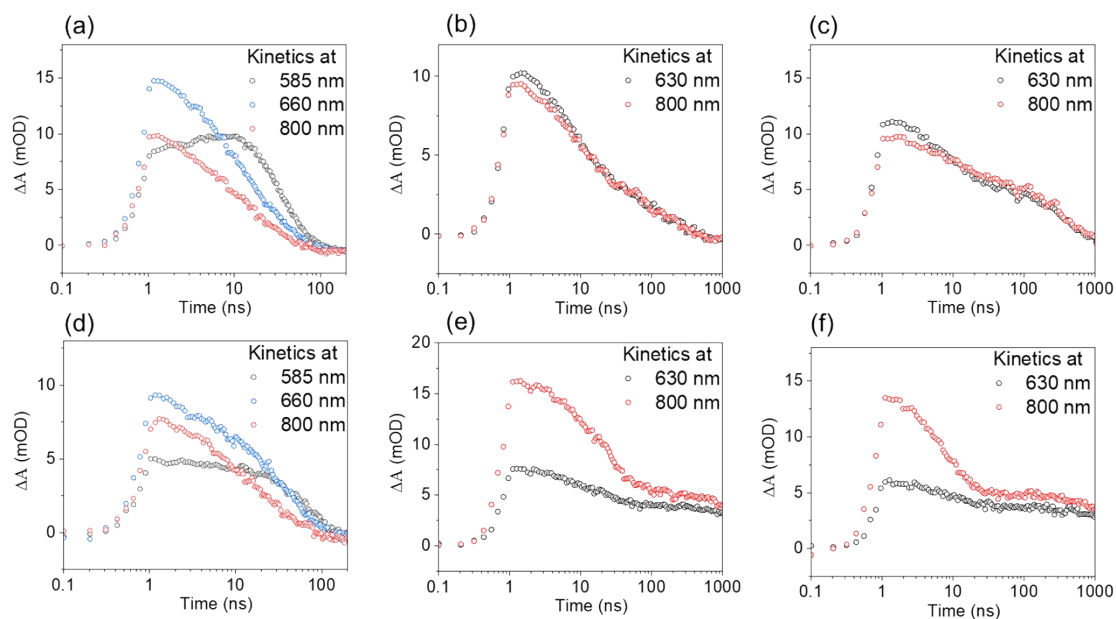


Figure S17. Kinetic fitting for (a) BP-*o*-Cz, (b) BP-*m*-Cz and (c) BP-*p*-Cz in THF and for (d) BP-*o*-Cz, (e) BP-*m*-Cz and (f) BP-*p*-Cz in DMF measured by ns-TA, purged by nitrogen.

Table S3. Lifetimes of BP-Cz dyads measured by ns-TA

		BP- <i>o</i> -Cz			BP- <i>m</i> -Cz		BP- <i>p</i> -Cz		
		τ [ns]	585 nm	660 nm	800 nm	630 nm	800 nm	630 nm	800 nm
THF	N ₂	τ_1	8.6±0.8	6.6±1.1	3.8±0.9	6.3±0.4	8.9±0.7	8.7±0.7	9.2±1.5
		τ_2	26.0±1.1	26.5±2.0	23.0±1.8	214±46	154±13	423±23	407.3±26
	O ₂	τ_1	8.5±1.3	6.7±1.3	5.1±1.1	6.6±4.5	4.9±0.8	5.0*	5.0*
		τ_2	21.8±1.5	24.3±2.8	23.6±3.0	22.8±2.5	24.0±2.2	27.3±0.9	27.1±1.0
DMF	N ₂	τ_1	5.9±2.0	1.5±0.6	6.8±1.6	15.6±1.4	20.9±0.9	8.6±1.9	7.4±0.4
		τ_2	62.5±4.1	40.6±1.7	38.1±4.9	3510±323	3091±353	3024±235	3830±386
	O ₂	τ_1	1.0*	0.5±0.3	0.4±0.5	12.4±1.9	10.9±2.7	5.0*	4.3±1.2
		τ_2	36.9±2.1	22.6±1.0	16.5±0.9	72.1±13	49.8±11	34.7±8.0	33.6±7.2

* Fix in kinetic fitting.

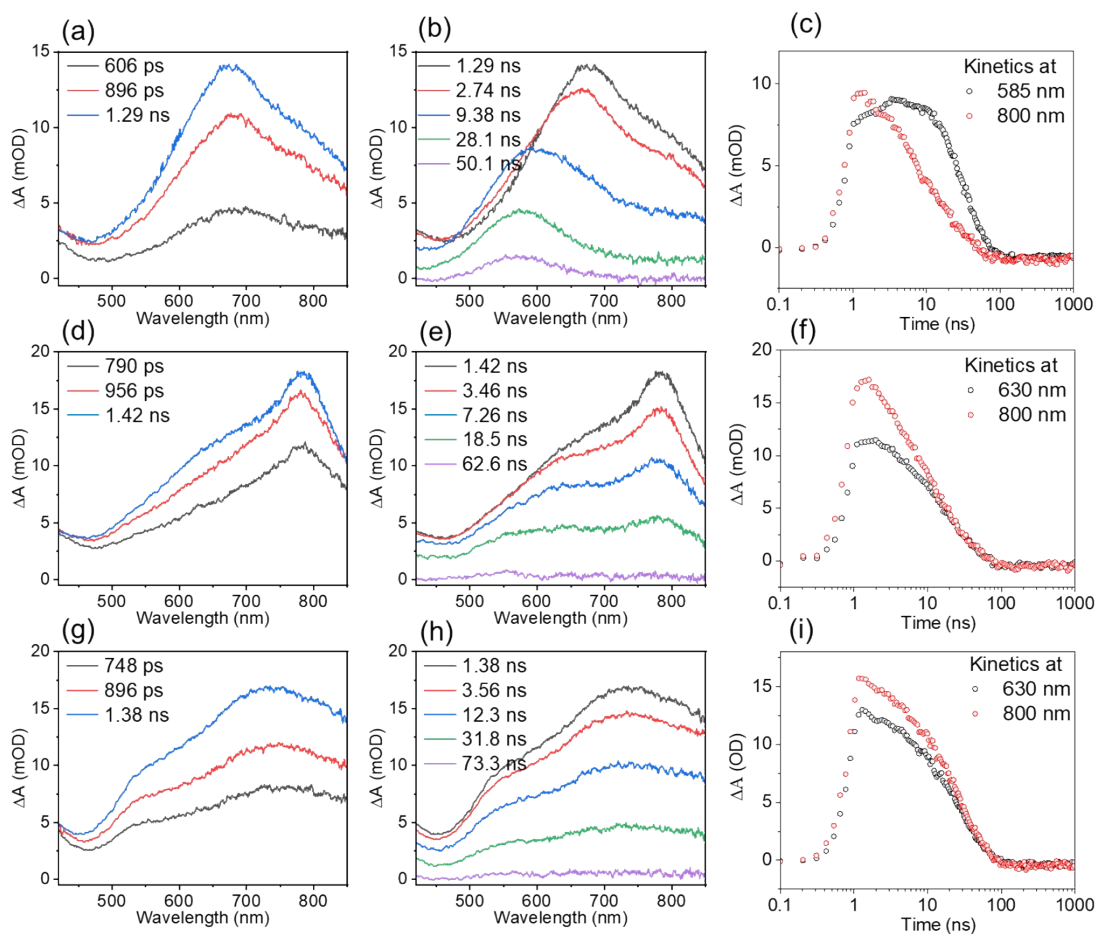


Figure S18. Ns-TA spectra and kinetic fitting of (a-c) BP-*o*-Cz, (d-f) BP-*m*-Cz and (g-i) BP-*p*-Cz in THF, 0.1 mM, purged by oxygen.

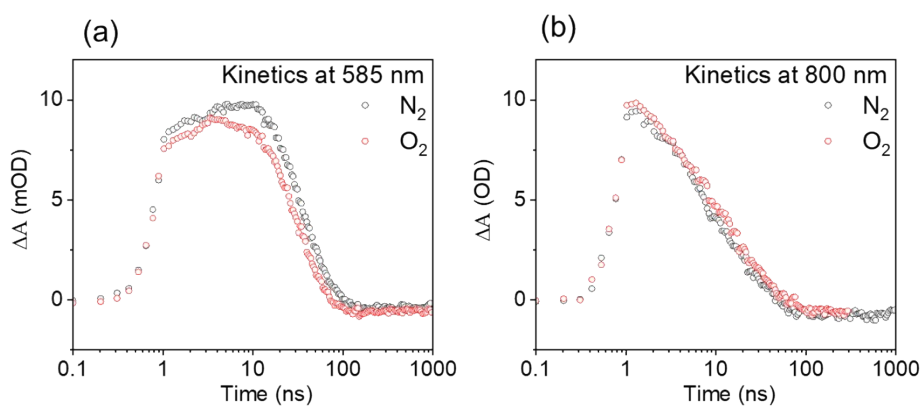
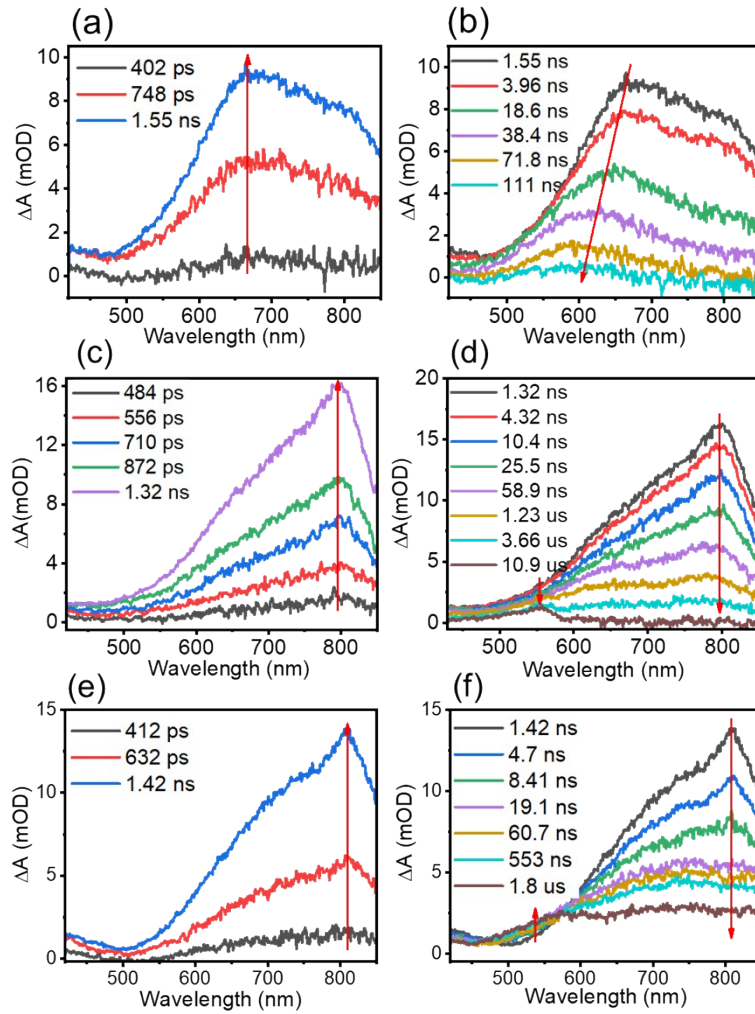


Figure S19. Kinetic fitting of BP-*o*-Cz under N₂ and O₂ conditions in THF, 0.1 mM.

Table S4. Quenching rate constant of BP-Cz dyads in ns-TA.

	BP- <i>o</i> -Cz			BP- <i>m</i> -Cz		BP- <i>p</i> -Cz		
	585 nm	660 nm	800 nm	630 nm	800 nm	630 nm	800 nm	
THF	$k_{N_2} (\times 10^7 s^{-1})$	3.85	3.77	4.35	0.47	0.65	0.24	0.25
	$k_{O_2} (\times 10^7 s^{-1})$	4.59	4.12	4.24	4.39	4.17	3.66	3.69
	$k_{quenched} (\times 10^7 s^{-1})$	0.74	0.34	-0.11	3.92	3.52	3.43	3.44
DMF	$k_{N_2} (\times 10^7 s^{-1})$	1.60	2.46	2.62	0.03	0.03	0.03	0.03
	$k_{O_2} (\times 10^7 s^{-1})$	2.71	4.42	6.06	1.39	2.01	2.88	2.98
	$k_{quenched} (\times 10^7 s^{-1})$	1.11	1.96	3.44	1.36	1.98	2.85	2.95

The k_{N_2} and k_{O_2} are calculated by the τ_2 from kinetic fitting measured by ns-TA, $k_{quenched}$ is calculated from the rate constant equation: $k_{N_2} + k_{quenched} = k_{O_2}$.

**Figure S20.** ns-TA spectra of (a, b) BP-*o*-Cz, (c, d) BP-*m*-Cz and (e, f) BP-*p*-Cz in DMF, 0.1 mM, purged by nitrogen.

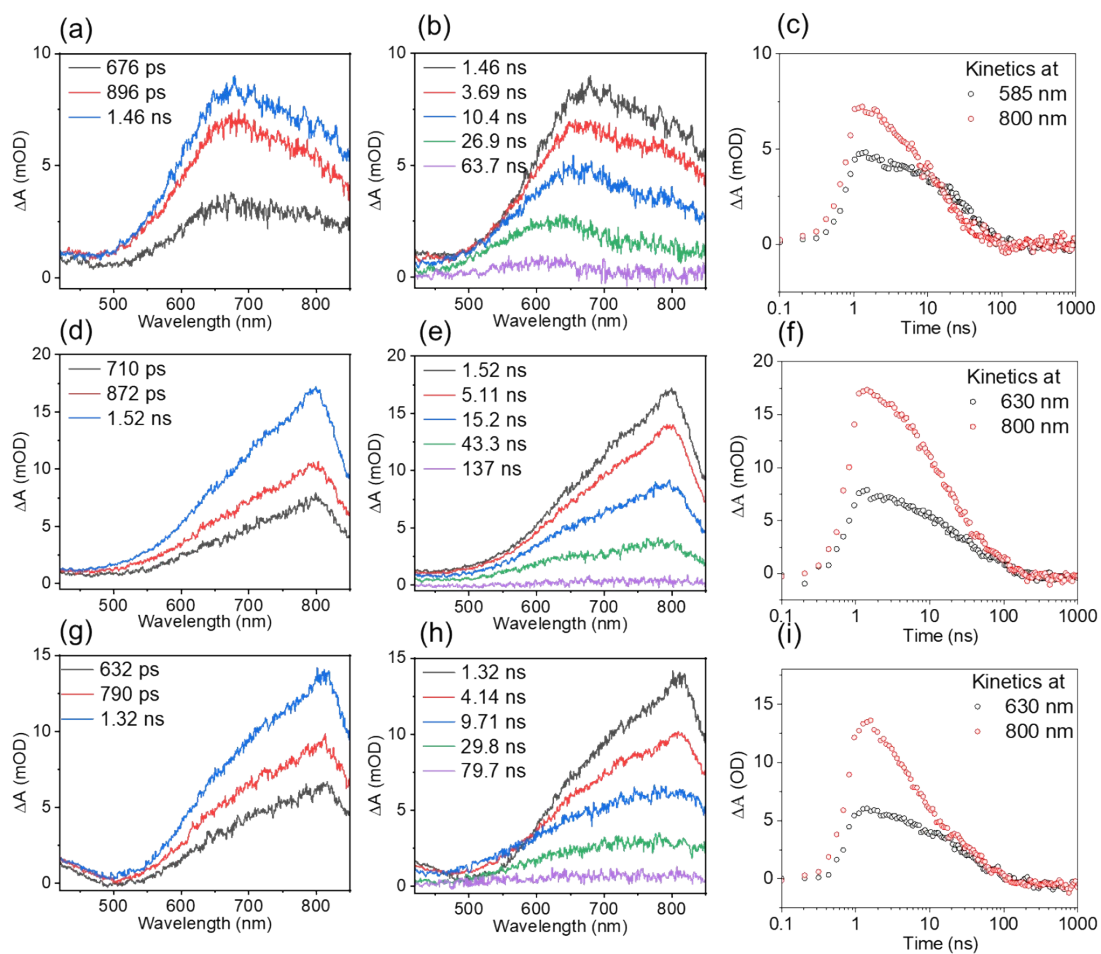


Figure S21. ns-TA spectra and kinetic fitting of (a-c) BP-*o*-Cz, (d-f) BP-*m*-Cz and (g-i) BP-*p*-Cz in DMF, 0.1 mM, purged by oxygen.

5. Theoretical calculations

Table S5. Oscillator strengths, Δr index and orbital contribution of S_1 and S_2 for BP-Cz dyads

	S_1			S_2		
	f	Δr (Å)	orbital contribution	f	Δr (Å)	orbital contribution
BP-<i>o</i>-BCz	0.0089	0.68	86-92 0.32 91-92 0.38	0.0183	1.95	91-92 0.57
BP-<i>m</i>-BCz	0.0012	0.831	84-92 0.43 88-92 0.45	0.0127	3.829	91-92 0.64
BP-<i>p</i>-BCz	0.0129	0.774	84-92 0.42 89-92 0.46	0.3437	3.524	91-92 0.62

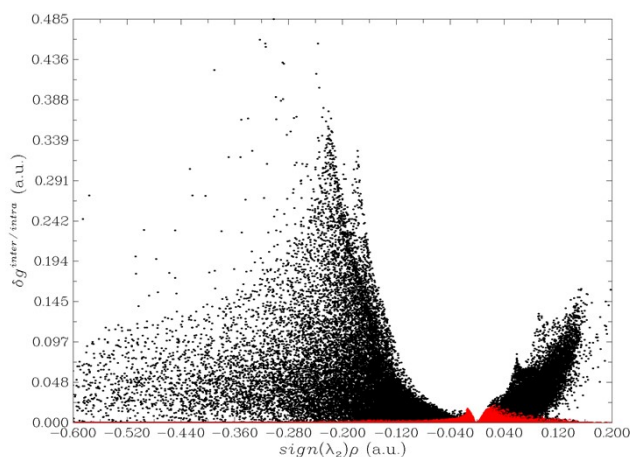


Figure S22. $\delta g^{\text{intra/inter}}$ vs $\text{sign}(\lambda_2)\rho$ of intermolecular interaction of BP-*o*-BCz

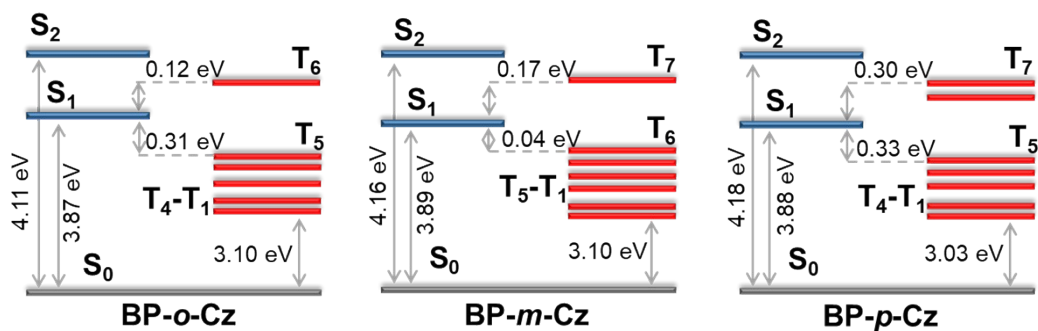


Figure S23. Excited-state energy level of BP-Cz dyads

Table S6. SOC constants related to S₁ and S₂ of BP-Cz dyads

BP- <i>o</i> -Cz	BP- <i>m</i> -Cz	BP- <i>p</i> -Cz
$\xi_{S_2-T_6} = 0.721 \text{ cm}^{-1}$	$\xi_{S_2-T_7} = 0.425 \text{ cm}^{-1}$	$\xi_{S_2-T_7} = 0.388 \text{ cm}^{-1}$
$\xi_{S_1-T_6} = 1.668 \text{ cm}^{-1}$	$\xi_{S_1-T_7} = 6.993 \text{ cm}^{-1}$	$\xi_{S_2-T_6} = 0.465 \text{ cm}^{-1}$
$\xi_{S_1-T_5} = 2.882 \text{ cm}^{-1}$	$\xi_{S_1-T_6} = 0.973 \text{ cm}^{-1}$	$\xi_{S_1-T_7} = 0.062 \text{ cm}^{-1}$
$\xi_{S_1-T_4} = 5.879 \text{ cm}^{-1}$	$\xi_{S_1-T_5} = 3.719 \text{ cm}^{-1}$	$\xi_{S_1-T_6} = 3.789 \text{ cm}^{-1}$
$\xi_{S_1-T_3} = 9.033 \text{ cm}^{-1}$	$\xi_{S_1-T_4} = 12.377 \text{ cm}^{-1}$	$\xi_{S_1-T_5} = 3.260 \text{ cm}^{-1}$
$\xi_{S_1-T_2} = 13.546 \text{ cm}^{-1}$	$\xi_{S_1-T_3} = 3.573 \text{ cm}^{-1}$	$\xi_{S_1-T_4} = 12.498 \text{ cm}^{-1}$
$\xi_{S_1-T_1} = 0.643 \text{ cm}^{-1}$	$\xi_{S_1-T_2} = 1.749 \text{ cm}^{-1}$	$\xi_{S_1-T_3} = 3.24 \text{ cm}^{-1}$
	$\xi_{S_1-T_1} = 15.971 \text{ cm}^{-1}$	$\xi_{S_1-T_2} = 0.116 \text{ cm}^{-1}$
		$\xi_{S_1-T_1} = 16.152 \text{ cm}^{-1}$
$\xi_{\text{Total}}: 34.372$	$\xi_{\text{Total}}: 45.780$	$\xi_{\text{Total}}: 39.970$

References

- [1] M. J. Frisch, G. W. Trucks, H. B. Schlegel, G. E. Scuseria, M. A. Robb, J. R. Cheeseman, G. Scalmani, V. Barone, G. A. Petersson, H. Nakatsuji, et al. *Gaussian 16 Rev. A.03*, Wallingford, CT, 2016.
- [2] T. Lu, F. Chen *J. Comput. Chem.* 2012, **33**, 580-592.
- [3] W. Humphrey, A. Dalke, K. Schulten *J. Mol. Graphics Modell.* 1996, **14**, 33-38
- [4] F. Neese *WIREs Computat. Mol. Sci.* 2017, **8**.